Supplementary Information (SI) for Journal of Materials Chemistry A.

Supporting Information

Synergistic Geometric and Electronic Modulation in Ni–Ce Layered Double Hydroxides for Enhanced Oxygen Evolution Reaction

Harish S. Chavan, Youngji Kim, Seungjoon Ha, Sangil Han, Seunghwa Lee*

Harish S. Chavan, Youngji Kim, Seungjoon Ha, Prof. Sangil Han, Prof. Seunghwa Lee
Department of Chemical Engineering Changwon National University, South Korea
E–mail: seunghwa@changwon.ac.kr

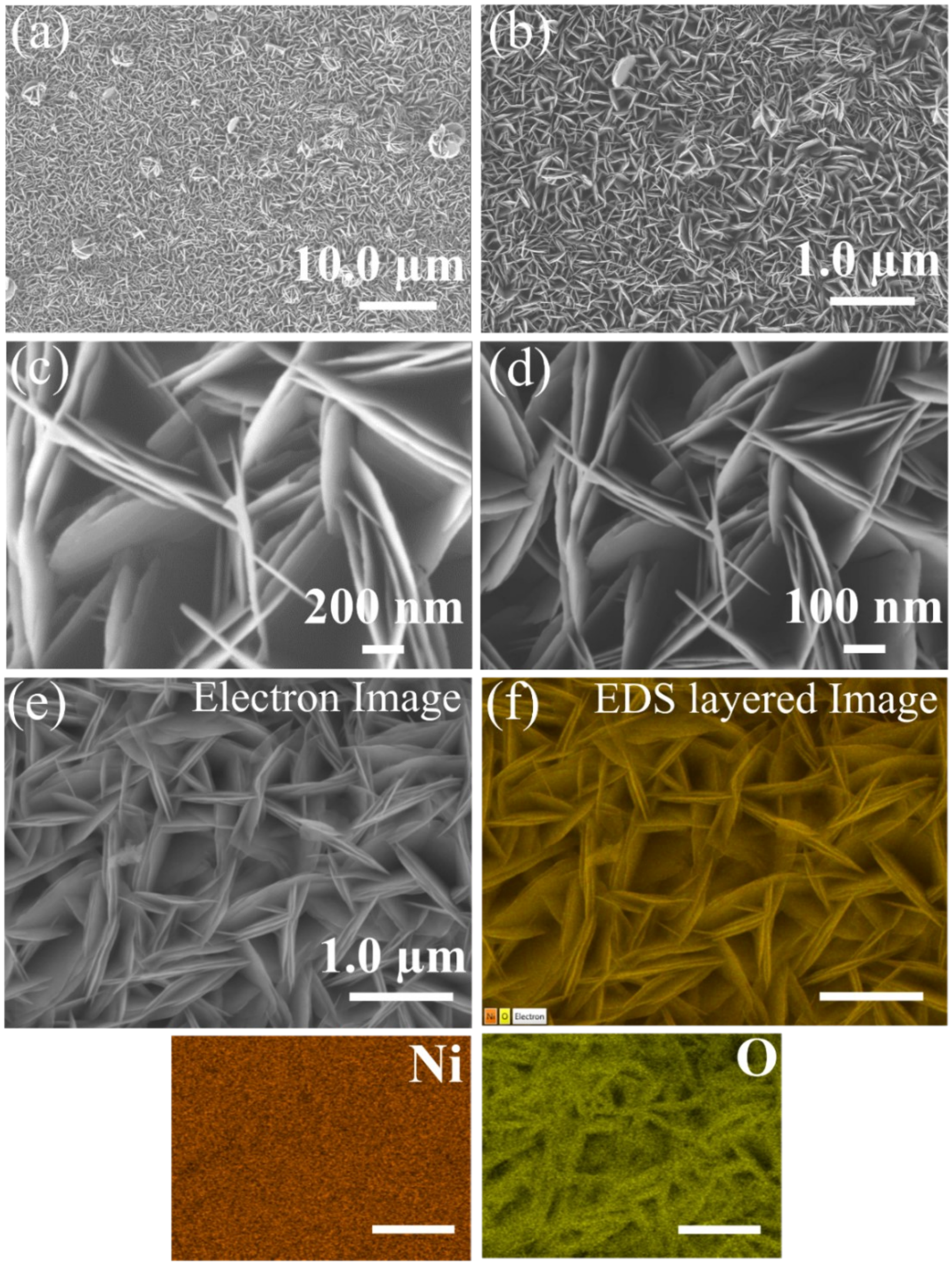

Figure S1. (a-d) Scanning electron microscopy (SEM) images, (e) Electron Images and (f) corresponding elements mapping of the $Ni_{1.0}$ hydroxide.

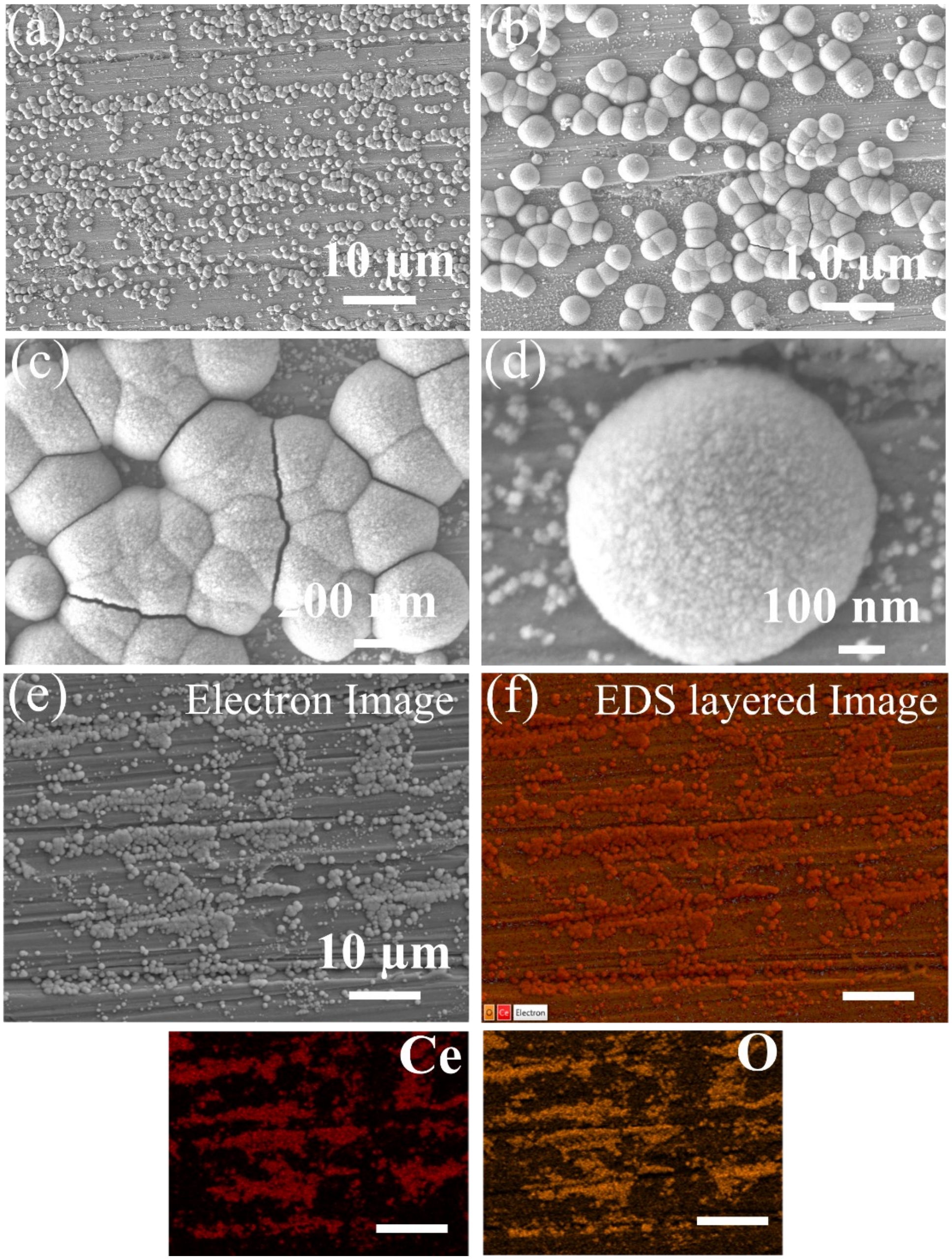

Figure S2. Scanning electron microscopy (SEM) images of (f) $Ce_{1.0}$ hydroxide,

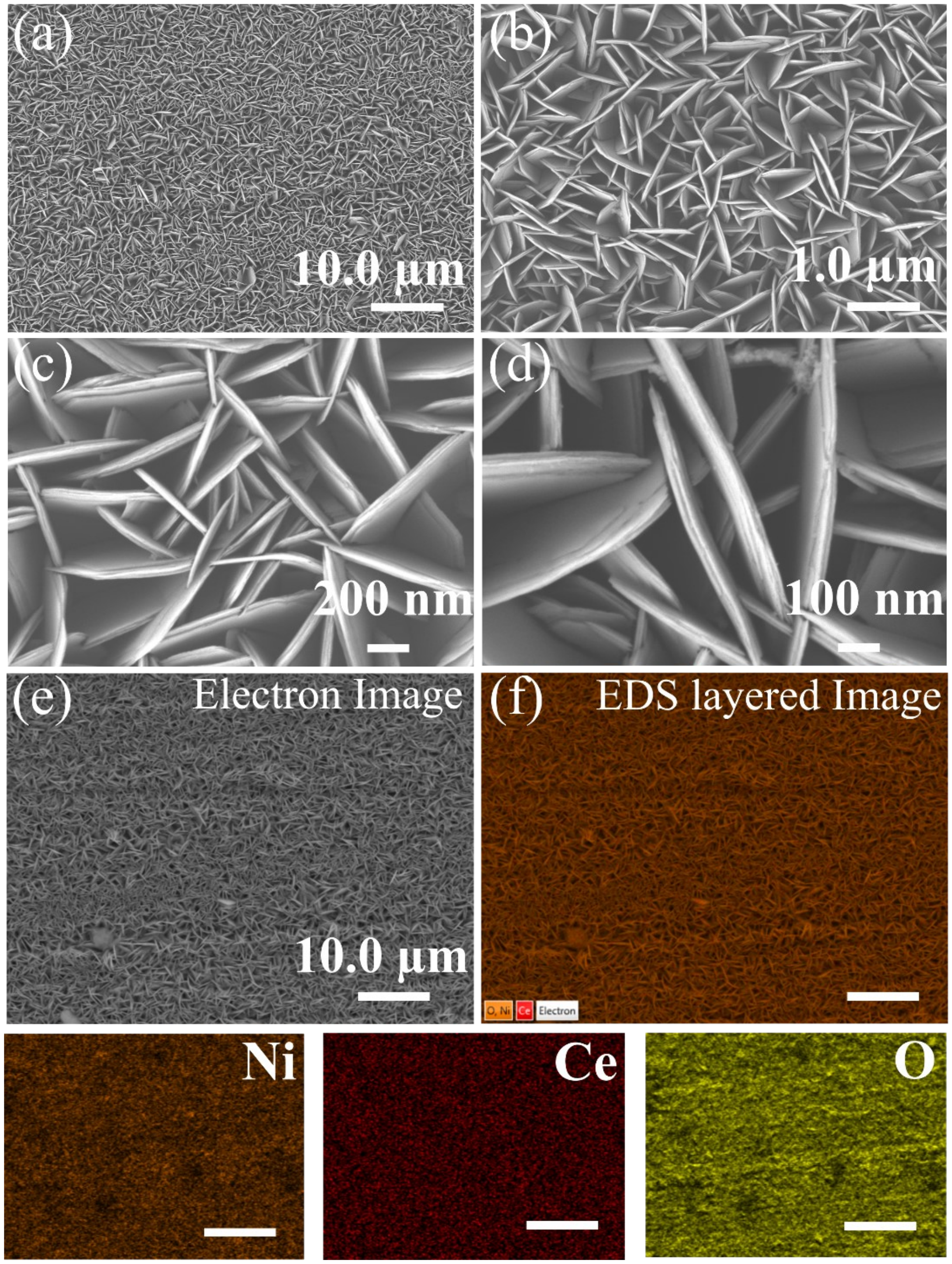

Figure S3. Scanning electron microscopy (SEM) images of (b) $Ni_{0.85}$ $Ce_{0.15}$ LDH, (f)The corresponding EDS elemental mapping.

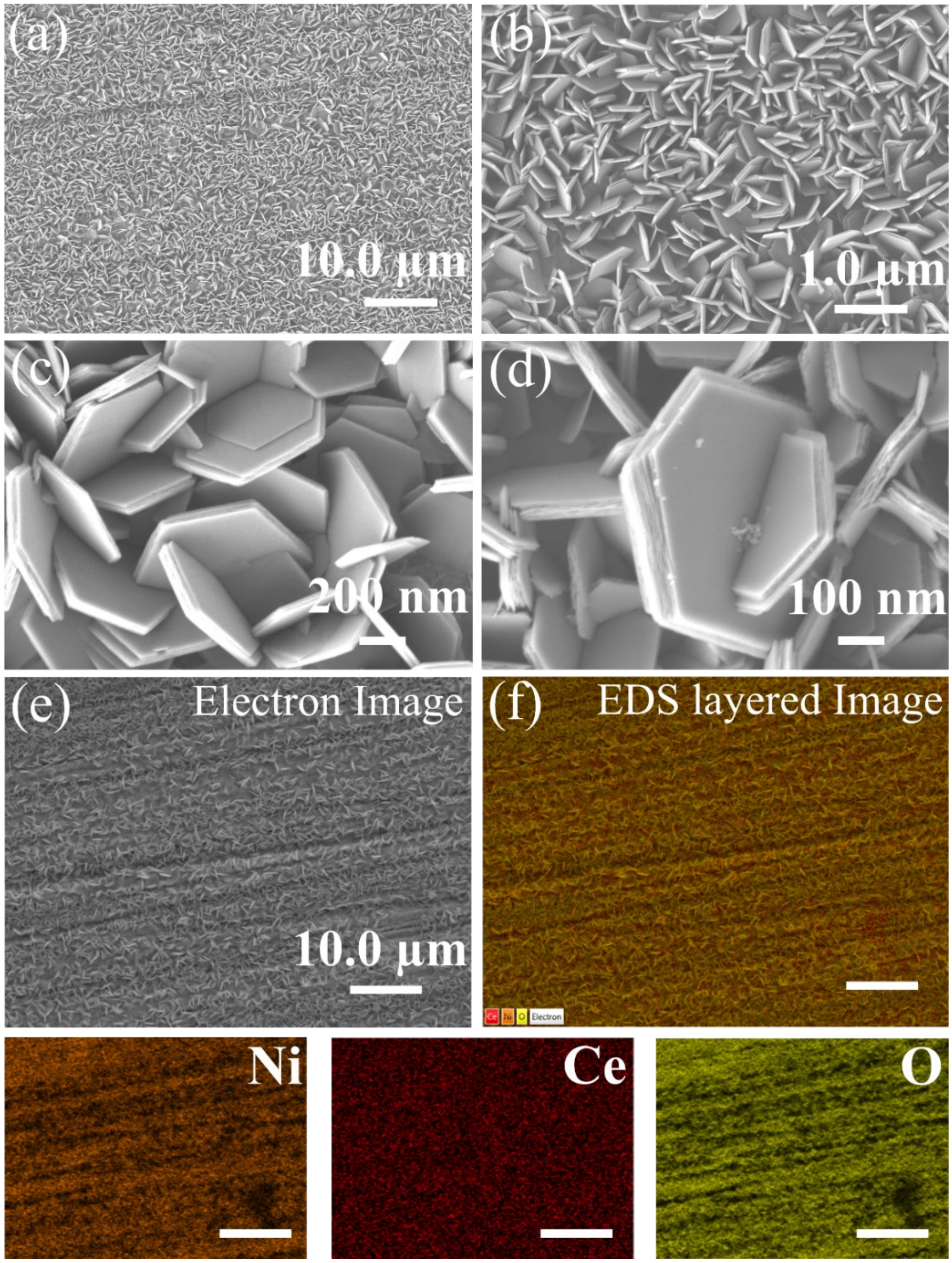

Figure S4. Scanning electron microscopy (SEM) images of (c) $Ni_{0.75}Ce_{0.25}$ LDH,

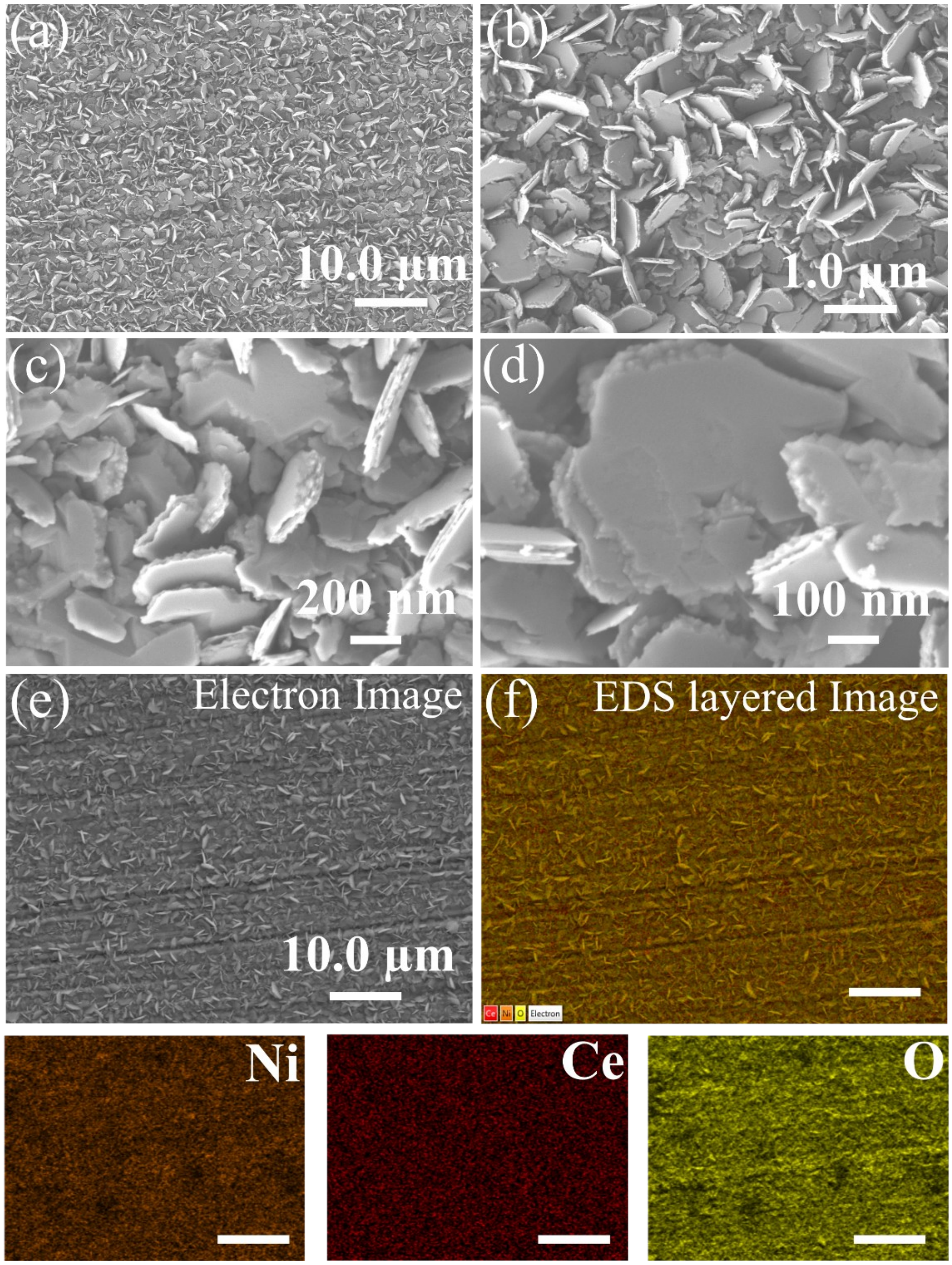

Figure S5. Scanning electron microscopy (SEM) images of (d) $Ni_{0.50}Ce_{0.50}$ LDH,

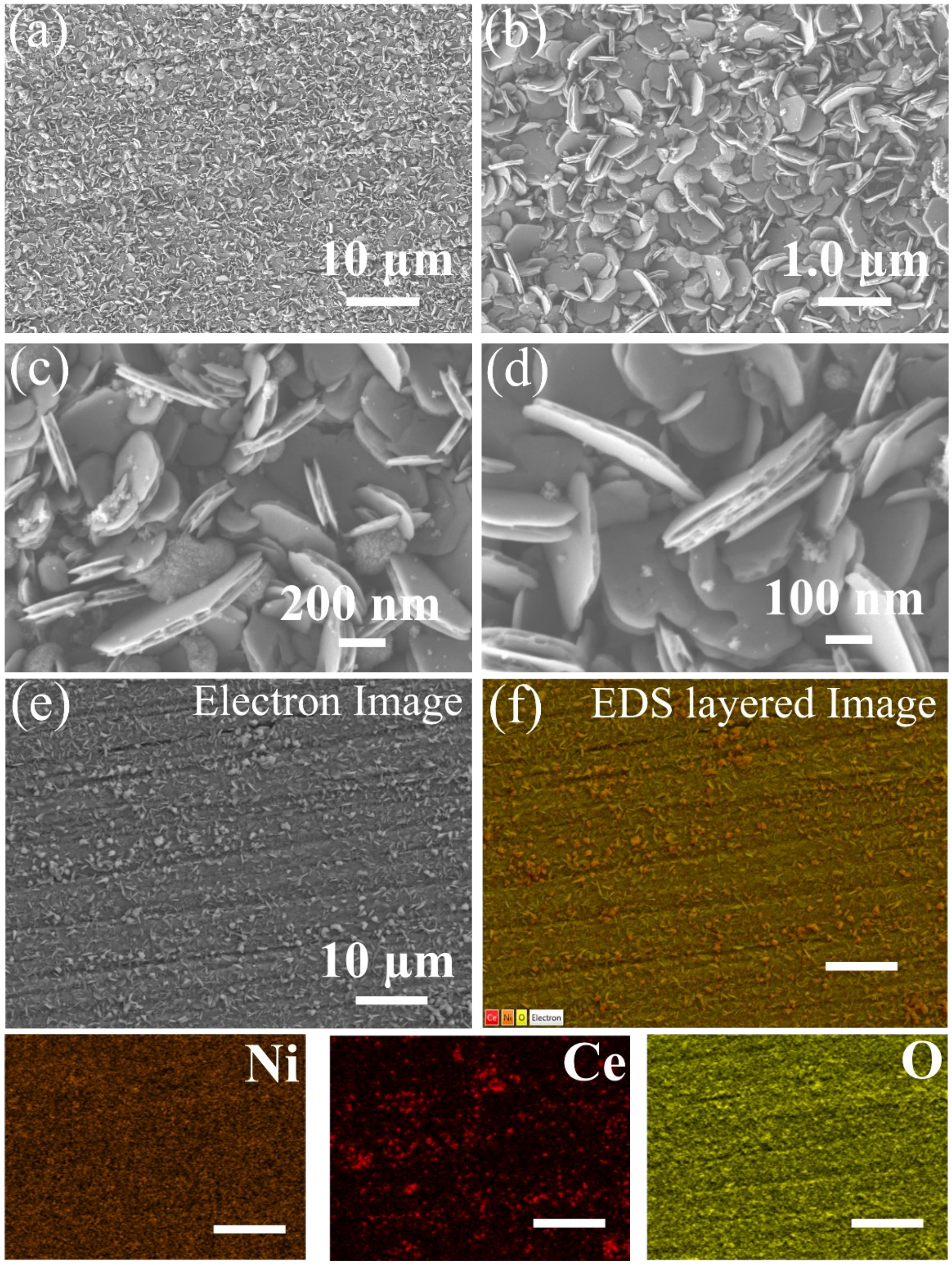

Figure S6. Scanning electron microscopy (SEM) images of (e) $Ni_{0.25}$ $Ce_{0.75}$ LDH,

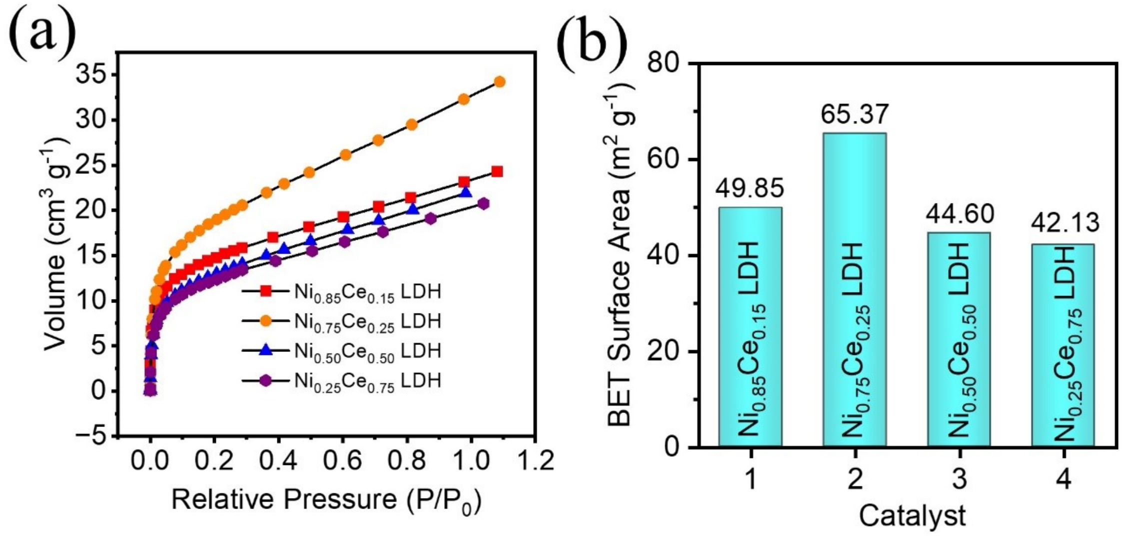

Figure S7. (a) BET adsorption isotherms, (b) Bar graph showing the measured surface areas of the different $Ni_{1-x}Ce_x$ LDH Ratios.

Samples	BET Surface area (m^2/g)	Total pore volume (cm^3g)	Average Pore diameter (nm)
Ni0.85Ce0.15 LDH	49.85	0.35	2.8884
Ni0.75Ce0.25 LDH	65.37	0.50	3.0778
Ni0.50Ce0.50 LDH	44.60	0.38	3.0399
Ni0.25Ce0.85 LDH	42.13	0.31	2.9763

Table-S1. BET surface areas and pore characteristics of the different $Ni_{1-x}Ce_x$ LDH Ratios.

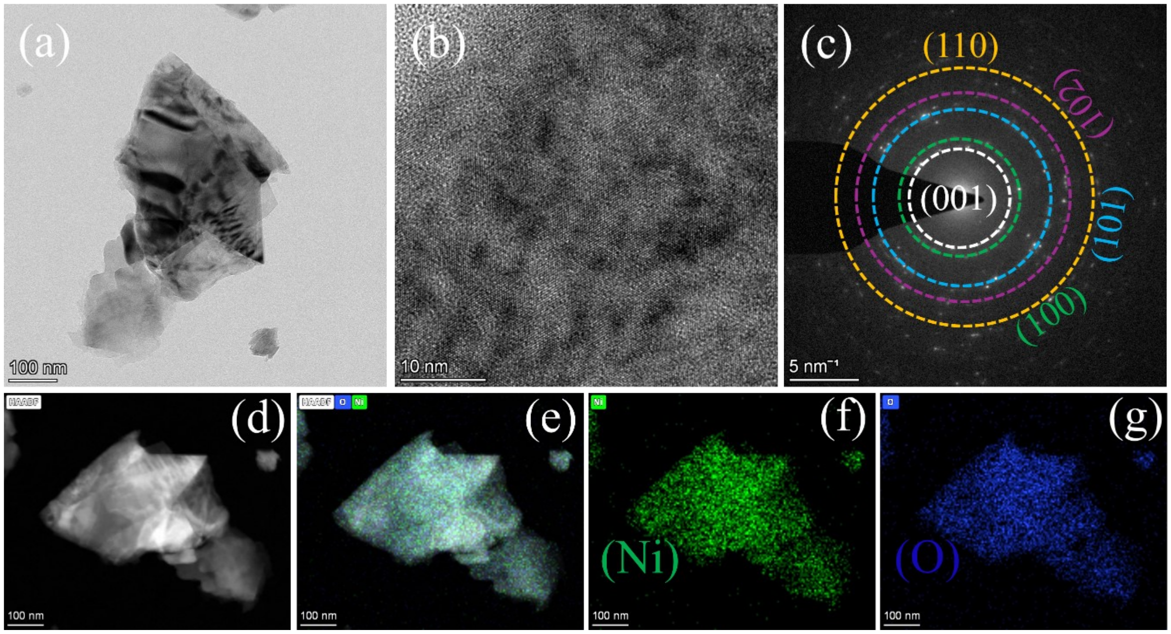

Figure S8. Transmission electron microscopy (TEM) images of $Ni(OH)_2$. **(a)** shows transmission electron microscopy (TEM) images of the interconnected $Ni(OH)_2$ nanosheets. **(b)** High-resolution TEM images of $Ni(OH)_2$. The appearance of bright spots without diffuse rings in the selective area electron diffraction (SAED) pattern in **(c)** confirms the formation of crystalline $Ni(OH)_2$, which is consistent with the X-ray diffraction (XRD) and TEM results. The high-angle annular dark field-scanning TEM (HAADF-STEM) and energy-dispersive X-ray (EDX) mapping images of a single nanosheet in (**d–g)** show the uniform distribution of Ni and O.

Table-S2. XRF analysis $Ni_{1-x}Ce_x$ LDH (where x = 0.15, 0.25, 0.50 and 0.75).

$Ni_{1-x}Ce_x$ LDH Ratios	**Compounds / Conc Unit**	**Ni**	**Ce**	**H_2O**
$Ni_{1.0}$	Conc Unit	54.3 ppm	-	99.995%
$Ni_{0.85}Ce_{0.15}$-LDH	Conc Unit	43.4ppm	6.2ppm	99.995%
$Ni_{0.75}Ce_{0.25}$-LDH	Conc Unit	59.5ppm	6.3ppm	99.993%
$Ni_{0.50}Ce_{0.50}$-LDH	Conc Unit	50.2ppm	7.2ppm	99.994%
$Ni_{0.25}Ce_{0.75}$-LDH	Conc Unit	20.5ppm	33.2ppm	99.995%
$Ce_{1.0}$	Conc Unit	-	265.9ppm	99.973%

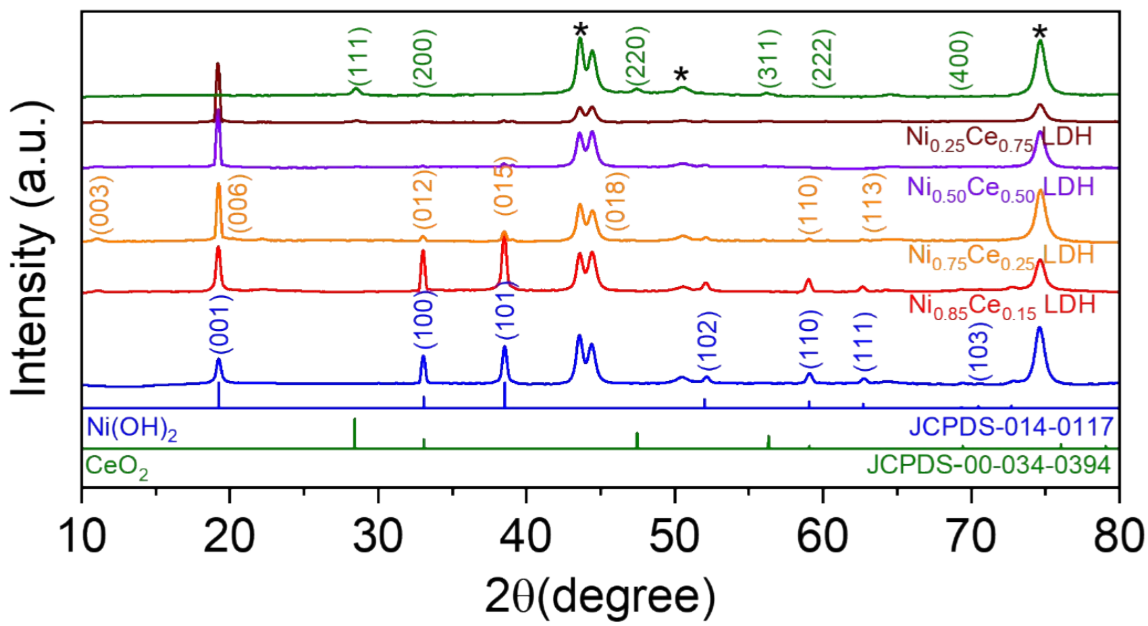

Figure S9. XRD of $Ni_{1-x}Ce_x$ LDH catalyst electrodes different Ni and Ce ratios, with Pure $Ni(OH)_2$ and CeO_2.

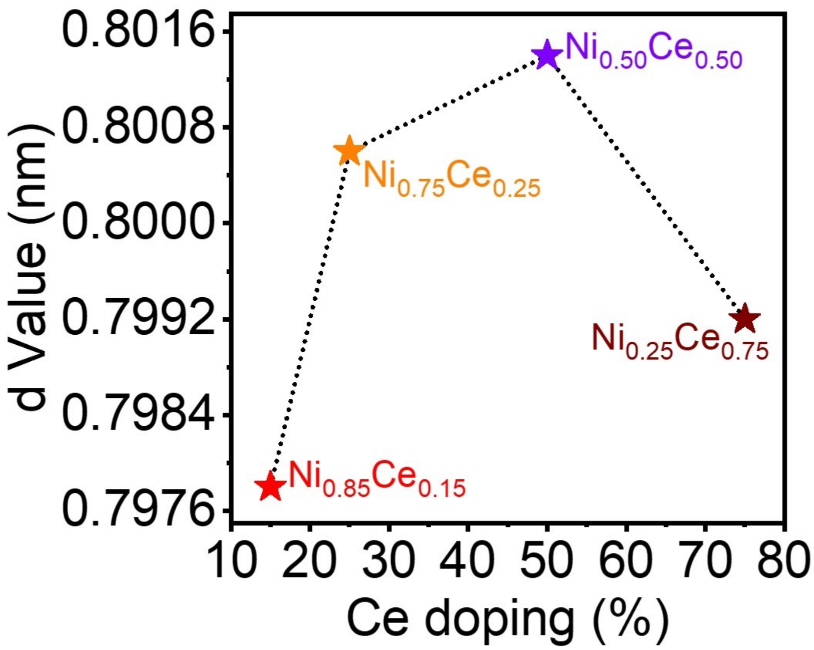

Figure S10. d-spacing values vs Ce doping (%) of $Ni_{1-x}Ce_x$-LDH ratios.

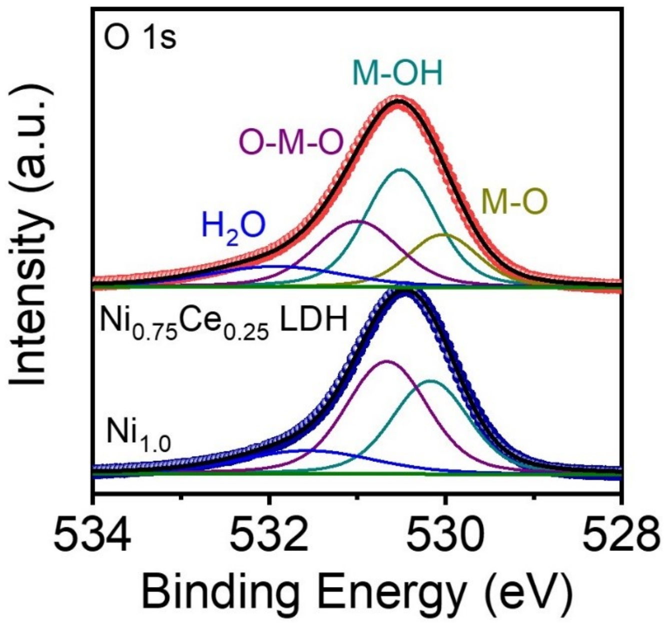

Figure S11. XPS O 1 s spectra of $Ni_{1.0}$ and $Ni_{0.75}Ce_{0.25}$-LDH.

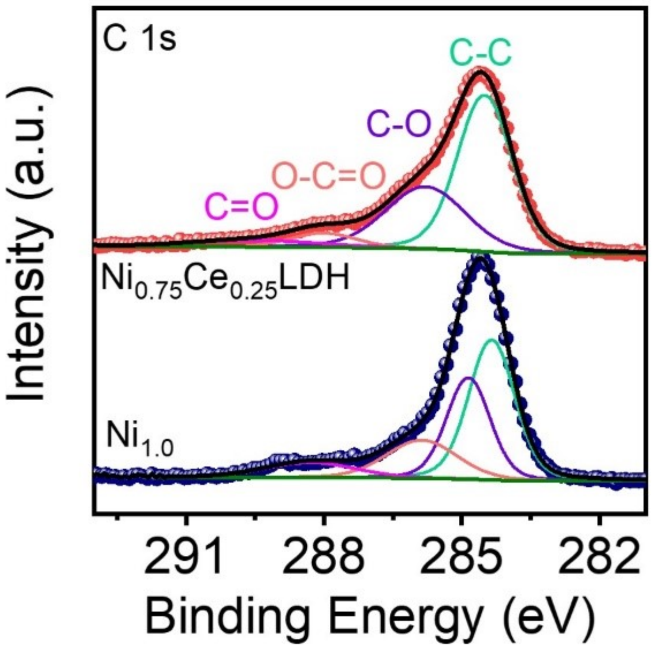

Figure S12. XPS C 1 s spectra of Ni1.0 and $Ni_{0.75}Ce_{0.25}$-LDH.

Table-S3. Electrochemical parameters obtained from LSV curves of the $Ni_{1-x}Ce_x$ LDH (where x = 0.15, 0.25, 0.50 and 0.75), $Ni_{1.0}$/SS, $Ce_{1.0}$/SS and S.S.

No	Catalyst	Overpotential (mV) @ 20 mA cm^{-2}	Overpotential (mV) @ 100 mA cm^{-2}	Tafel mV dec^{-1}	mF cm^{-2}	ECSA=cm^2
1	$Ni_{1.0}$	269	336	99.19	1.5994	39.98
2	$Ni_{0.85}Ce_{0.15}$LDH	260	329	75.83	1.8430	46.08
3	$Ni_{0.75}Ce_{0.25}$LDH	220	278	61.11	3.4143	85.36
4	$Ni_{0.50}Ce_{0.50}$LDH	258	320	90.5	1.9591	48.98
5	$Ni_{0.25}Ce_{0.75}$LDH	262	323	77.21	2.4381	60.95
6	$Ce_{1.0}$	306	358	81.16	2.0982	52.46
7	SS	354	-	177.95	-	-

Table S4. Comparison of OER activity of the Ni0.75Ce0.25 LDH with some other reported LDH catalysts.

No	**Electrocatalysts**	**Overpotential (mV) @10,20 mA cm^{-2}**	**Tafel slope (mV dec^{-1})**	**References**
	$Ni_{0.75}Ce_{0.25}$ LDH	220 @20 mA cm^{-2}	61.11	This Work
1	Ni_4Ce_1	220@10	81.9	ACS Nano 2018, 12, 6245−6251
2	$NiCeO_x$	295@10	66	ACS Catal. 2019, 9, 1605−1611
3	$CeO_2/CoSe_2$	290@10	41	Small, 2015, 11, 182-188.
4	CeO_2: 3D $CeO_2/Ni(OH)_2$	240@10	57	Chem. Sci.,2017, 8,3211
5	Ir-CeO_2-C	279@10	48.3	*Nano Research.* **2022**, 16, 7724
6	Ru/d-NiFe LDH	224@10	60.48	*Adv. Energy Mater.* **2024***, 14, 2400059*
7	NiFe-LDH	239@10	53	ACS Appl. Mater. Interfaces 2016, 8, 33697−33703
8	$Ni_{0.75}V_{0.25}$-LDH	310@10	50	Nat. Commun. 2016, 7, 11981.
9	NiFeCe-LDH	232@10	31.69	Chemical Engineering Journal 464 (2023) 142669
10	CoFeRu-LDH	297@10	75	**https://doi.org/10.1002/smll.202502821**
11	NiFeCe-LDH	267@10	31.7	Chem. Eng. J. 2023, 464, 142669.
12	MXene/NiCo-LDH	310@10	43	Sustainable Energy & Fuels 2023, 7, 4638.
13	NiCo-LDH	314@10	77	ACS Applied Energy Materials 2019, 2, 312.
14	NiCoFe-LDH	340@10	93	Advanced Energy Materials 2015, 5, 1500245.
15	CoCr LDH	340@10	81	J. Mater. Chem. A, 2016, 4,11292-11298
16	MOF-74-derived NiFe LDH	299@10	48.7	Chemical Engineering Journal 2021, 423, 130204.
17	CoFe-LDH/rGO	325@10	43	Advanced Materials Interfaces 2016, 3, 1500782.
18	$Co_{0.4}Fe_{0.6}$ LDH	280@10	29	ACS Appl Energy Mater 2018,1,1200–9.
19	NiFeCoLDH	249@10	42	Small 2020,16, e2002426
20	NiFeCe-LDH	227@10	33	ACS Appl Mater Interfaces 2018,10,6336–45.
21	Au/NiFe LDH	237@10	37	J Am Chem Soc 2018,140, 3876–9.

22	CoV-LDHs	250@10	44	Energy Environ. Sci.2018, 11, 1736
23	NiFe-LDHs	270@10	48.6	Int. J. Hydrogen Energy 2022, 47, 23498.
24	$NiCo_1 Fe_1$ -LDHs	231@10	59	Int. J. Hydrogen Energy 2022, 47, 23644.

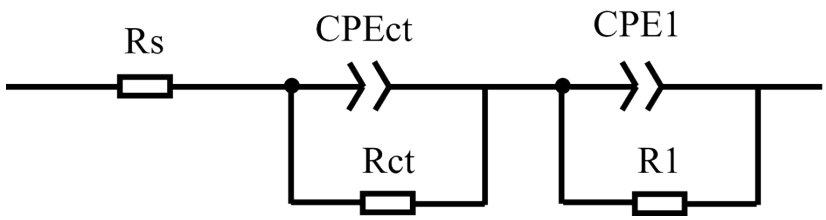

Figure S13. Equivalent circuit diagram used to fit the Nyquist plot of the $Ni_{1-x}Ce_x$ LDHs.

Table-S5. The physical parameters obtained by Equivalent circuit model for EIS data fitting the Nyquist plots of $Ni_{1.0}$/S.S, $Ni_{0.85}Ce_{0.15}$-LDH/S.S., $Ni_{0.75}Ce_{0.25}$-LDH/S.S., $Ni_{0.50}Ce_{0.50}$-LDH/S.S., $Ni_{0.25}Ce_{0.75}$-LDH and $Ce_{1.0}$/S.S.

No	Catalyst	$R_s(\Omega)$	CPS_{ct}	$R_{ct}(\Omega)$	CPS_1	$R_1(\Omega)$
1	$Ni_{1.0}$	1.305	0.0179	1.639	0.0301	0.3278
2	$Ni_{0.85}Ce_{0.15}LDH$	1.318	0.01942	0.9205	0.1004	0.3535
3	$Ni_{0.75}Ce_{0.25}LDH$	1.131	0.00641	0.1516	0.115	0.436
4	$Ni_{0.50}Ce_{0.50}LDH$	1.153	0.02262	0.308	0.02378	0.92
5	$Ni_{0.25}Ce_{0.75}LDH$	0.273	0.41	1.774	0.01876	1.13
6	$Ce_{1.0}$	0.9065	0.006364	2.059	0.03669	0.3422
7	S.S.	1.112	0.002684	15.87	0.0504	0.9935
8	$Ni_{0.75}Ce_{0.25}LDH$ After 265 h stability	1.188	0.2968	0.2582	0.04578	1.278

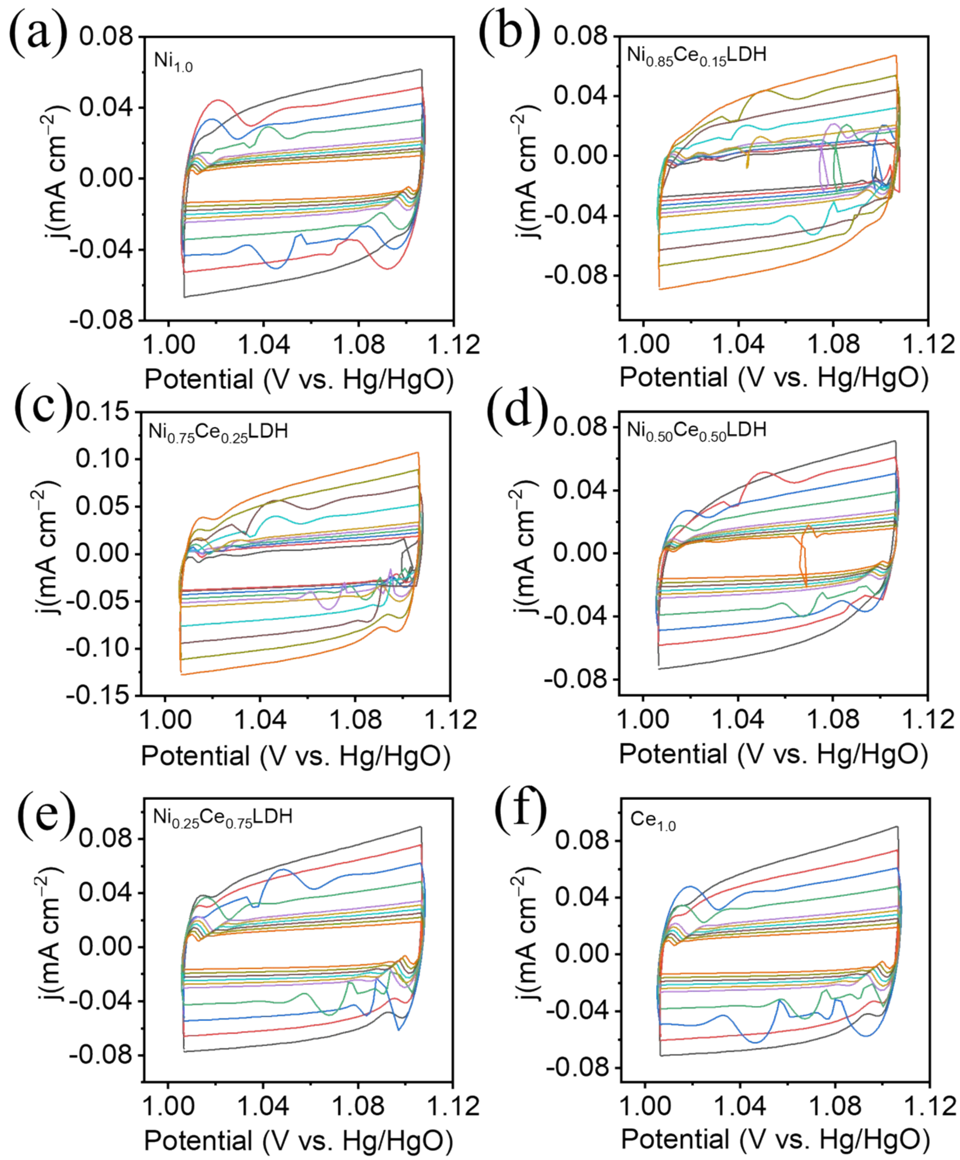

Figure S14. The non-Faradic current density based electrochemically active surface area. (ECSA) of $Ni_{1.0}$ hydroxide, and $Ni_{0.85}V_{0.15}$ layered double hydroxide (LDH), $Ni_{0.75}V_{0.25}$ LDH, $Ni_{0.50}V_{0.50}$ LDH, $Ni_{0.25}V_{0.75}$ LDH and $Ce_{1.0}$ hydroxide.

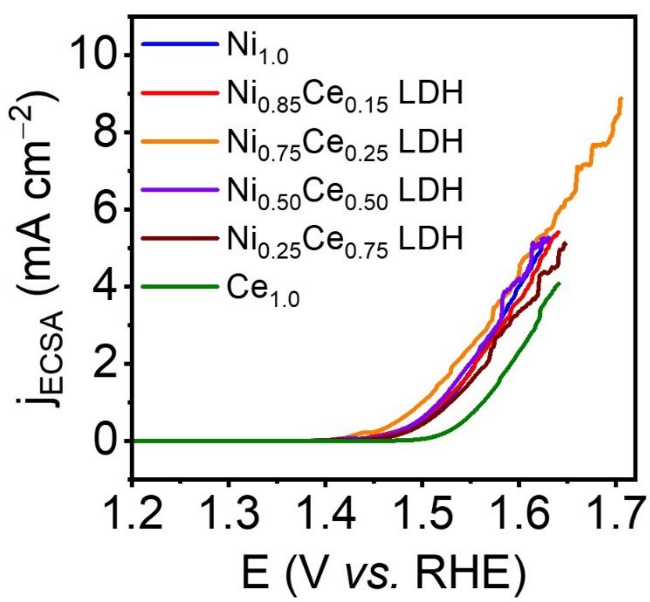

Figures S15. ECSA-normalized polarization curve graph.

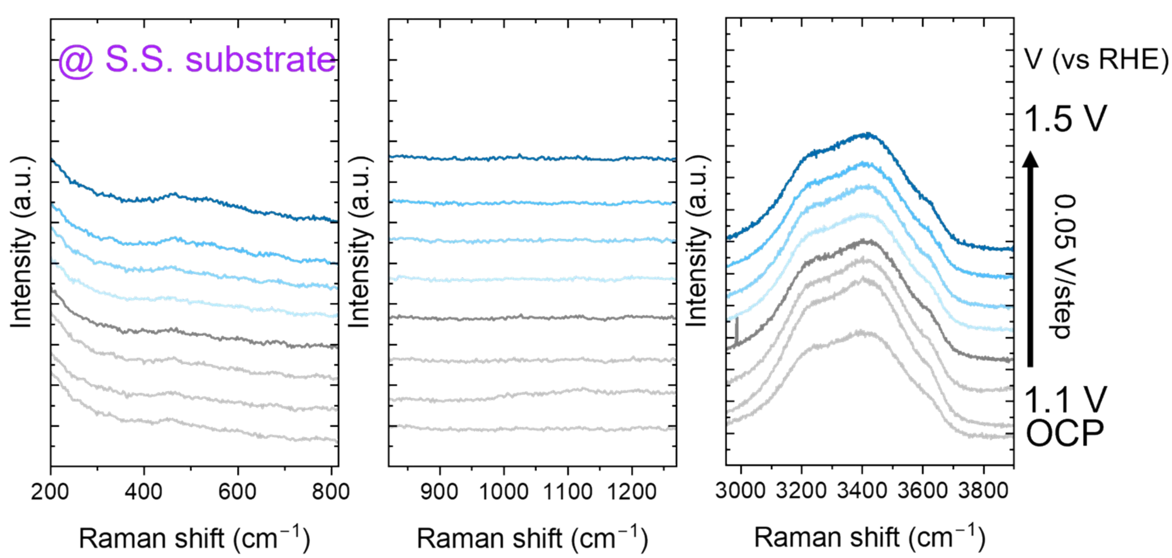

Figures S16. Potential-dependent in situ Raman spectra of Stainless-Steel Substrate (S.S.) in 1.0 M KOH.

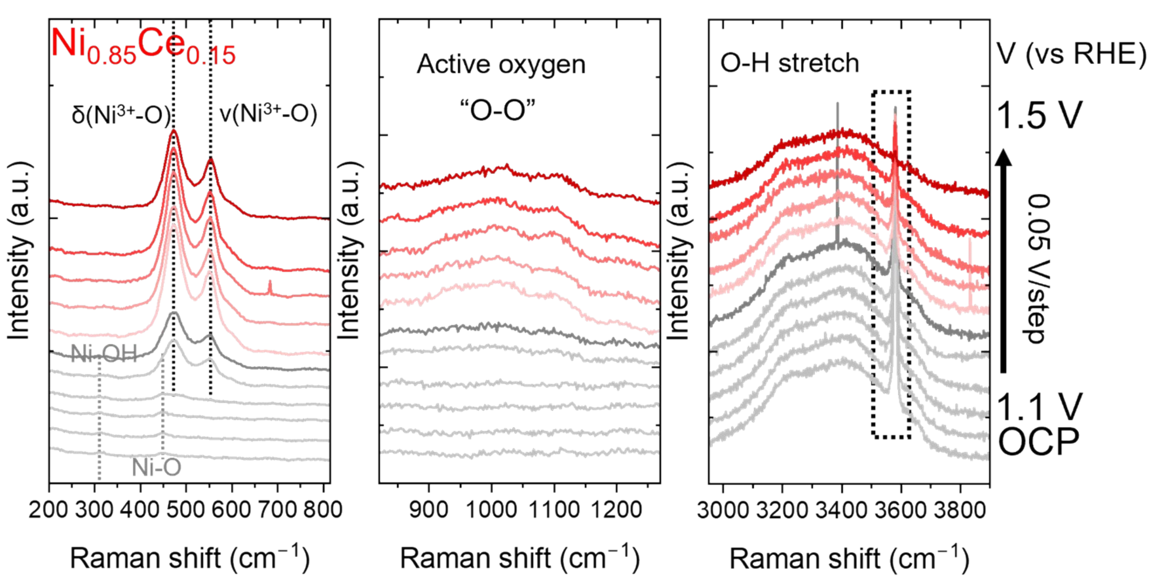

Figures S17. Potential-dependent in situ Raman spectra of $Ni_{0.85}Ce_{0.15}$-LDH in 1.0 M KOH

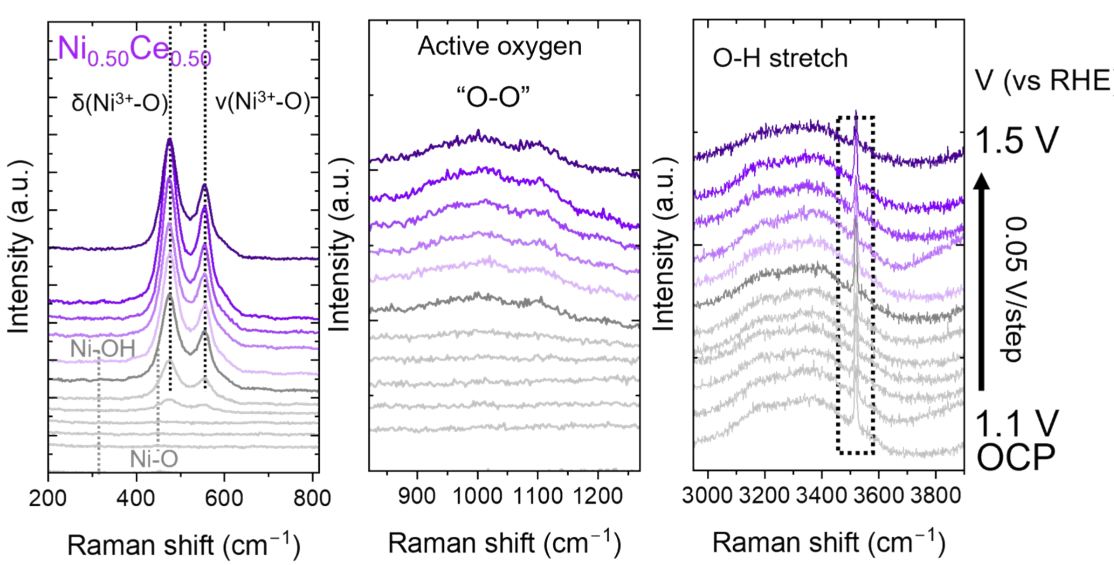

Figures S18. Potential-dependent in situ Raman spectra of $Ni_{0.50}Ce_{0.50}$ -LDH in1.0 M KOH

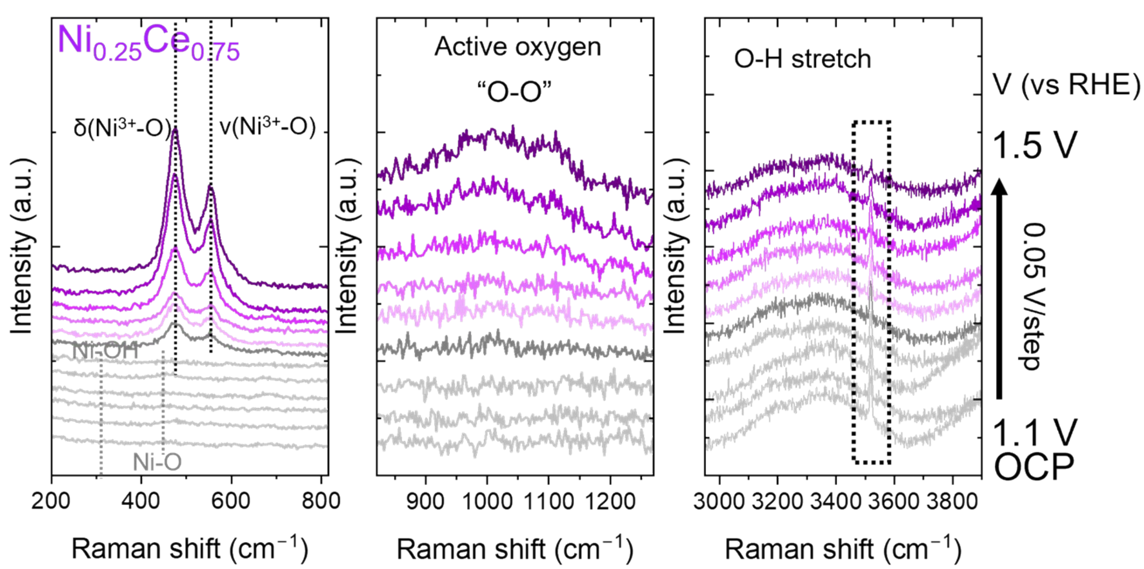

Figures S19. Potential-dependent in situ Raman spectra of $Ni_{0.25}Ce_{0.75}$ -LDH in1.0 M KOH

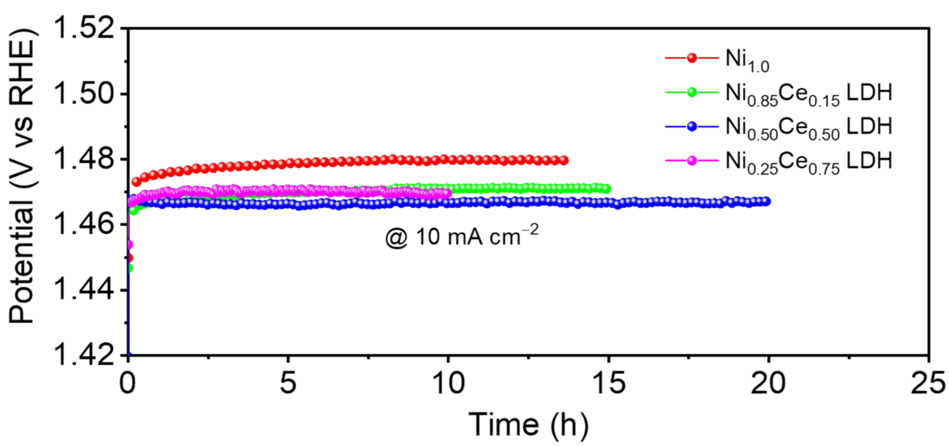

Figures S20. Stability performances of the $Ni_{1.0}$-LDH, $Ni_{0.85}Ce_{0.15}$-LDH, $Ni_{0.50}Ce_{0.50}$-LDH and $Ni_{0.25}Ce_{0.75}$-LDH at 10 mA cm^{-2} in 1.0 M KOH.

Table-S6. XRF analysis of $Ni_{0.75}Ce_{0.25}$-LDH Pristine and after 265 h stability test.

NiCe-LDH Ratios	Compounds / Conc Unit	Ni	Ce	H_2O
Pristine-$Ni_{0.75}Ce_{0.25}$ LDH	Conc Unit	59.5ppm	6.3ppm	99.993%
After 265 h stability-$Ni_{0.75}Ce_{0.25}$ LDH	Conc Unit	59.6ppm	4.5ppm	99.994%

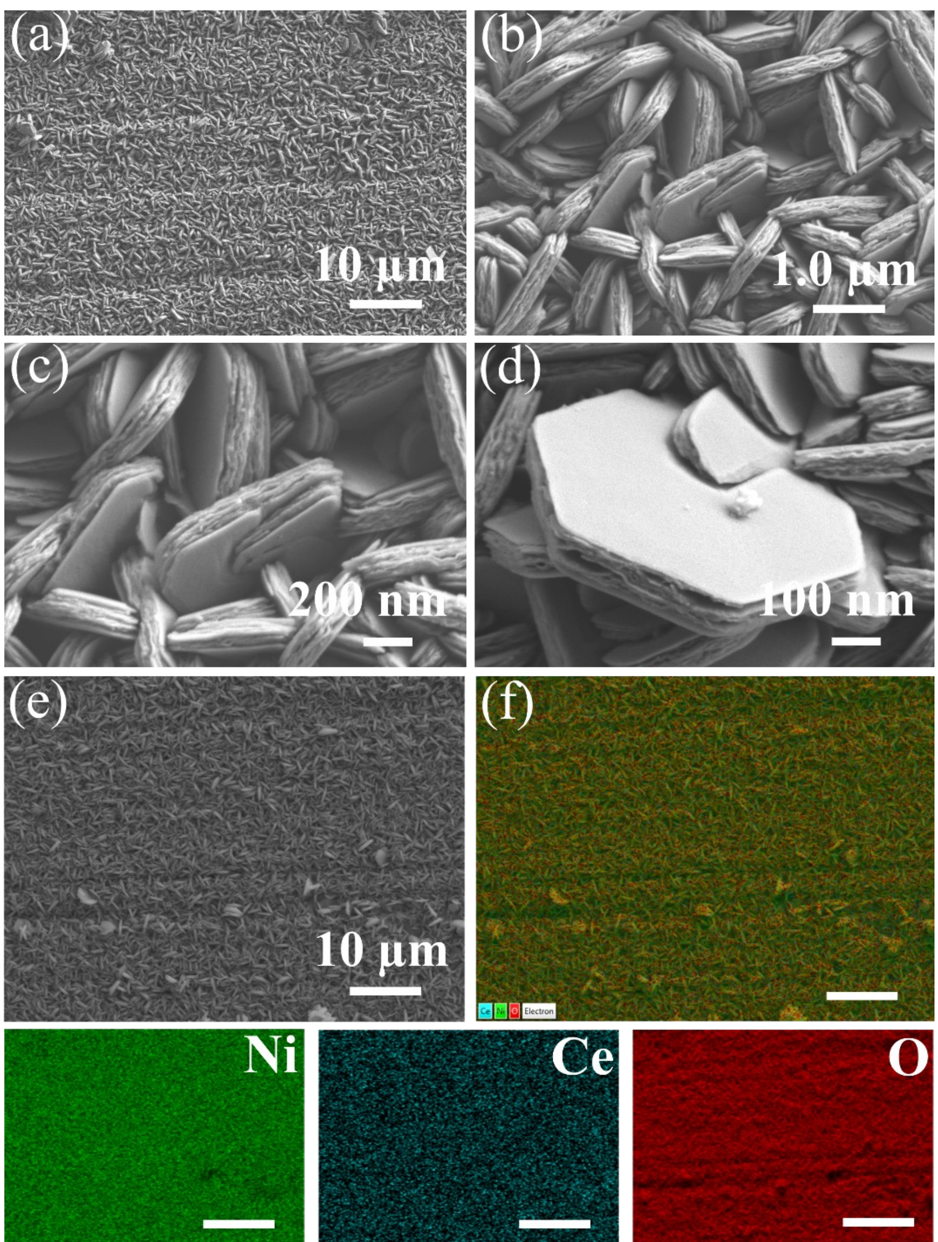
(a)
10 µm
(b)
1.0 µm
(c)
200 nm
(d)
100 nm
(e)
10 µm
(f)
Ni
Ce
O

Figure S21. Scanning electron microscopy (SEM) images of After 265 h stability $Ni_{0.75}$ $Ce_{0.25}$ LDH

References

1. D. Zhao, Y. Pi, Q. Shao, Y. Feng, Y. Zhang, X. Huang, Enhancing Oxygen Evolution Electrocatalysis via the Intimate Hydroxide-Oxide Interface, ACS Nano **12 (2018)** 6245−6251.

2. J. Yu, Q. Cao, Y. Li, X. Long, S. Yang, J. K. Clark, M. Nakabayashi, N. Shibata, J.-J. Delaunay, Defect-Rich NiCeOx Electrocatalyst with Ultrahigh Stability and Low Overpotential for Water Oxidation, ACS Catal. 9 (2019**)** 1605−1611.

3. Y. R. Zheng, M. R. Gao, Q. Gao, H. H. Li, J. Xu, Z. Y. Wu, S. H. Yu, An Efficient CeO_2/$CoSe_2$ Nanobelt Composite for Electrochemical Water Oxidation, Small, 11 (2015) 182−188.

4. Z. Liu, N. Li, H. Zhao, Y. Zhang, Y. Huang, Z. Yinde, Y. Du, Regulating the active species of $Ni(OH)_2$ using CeO_2: 3D $CeO_2/Ni(OH)_2$/carbon foam as an efficient electrode for the oxygen evolution reaction, Chem. Sci.8 (2017) 3211−3217.

5. X. Chen, W. Liao, M. Zhong, J. Chen, S. Yan, W. Li, C. Wang, W. Chen, X. Lu, Rational design of robust iridium-ceria oxide-carbon nanofibers to boost oxygen evolution reaction in both alkaline and acidic media, Nano Research. 16 (**2022)** 7724−7732.

6. Y. Chen, Y. Liu, W. Zhai, H. Liu, T. Sakthivel, S. Guo, Z. Dai, Metastabilizing the Ruthenium Clusters by Interfacial Oxygen Vacancies for Boosted Water Splitting Electrocatalysis, Adv. Energy Mater. 14 (2024) 2400059.

7. C. Zhang, M. Shao, L. Zhou, Z. Li, K. Xiao, M. Wei, Hierarchical NiFe Layered Double Hydroxide Hollow Microspheres with Highly-Efficient Behavior toward Oxygen Evolution Reaction, ACS Appl. Mater. Interfaces 8 (2016) 33697−33703.

8. K. Fan, H. Chen, Y. Ji, H. Huang, P. M. Claesson, Q. Daniel, B. Philippe, H. Rensmo, F. Li, Y. Luo, L. Sun, Nickel–vanadium monolayer double hydroxide for efficient electrochemical water oxidation, Nat. Commun. 7 (2016) 11981.

9. Y. Liao, R. He, W. Pan, Y. Li, Y. Wang, J. Li, Y. Li, Lattice distortion induced Ce-doped NiFe-LDH for efficient oxygen evolution, Chem. Engin. J. 464 (2023) 142669.

10. S. Jung, R. A. Senthil, C. J. Moon, A. Kumar, M. Ubaidullah, M. Y. Choi, Laser-Regulated CoFeRu-LDH Nanostructures: Nitrite-to-Ammonia Production in Zn–Nitrite Battery and Oxygen Evolution in Water Electrolysis, Small 21 (2025) 2502821.

11. Y. Liao, R. He, W. Pan, Y. Li, Y. Wang, J. Li, Y. Li, Lattice distortion induced Ce-doped NiFe-LDH for efficient oxygen evolution, Chem. Engin. J. 2023, 464, 142669.

12. B. Vishnu, S. Srirama, J. Jayabharathi, A green synthetic approach: crystalline–amorphous interface CoFe-LDH as a sustainable electrocatalyst for water oxidation with low cell voltage and evaluation of its sustainability standards, Sustainable Energy & Fuels 2023, 7, 4638−4653.

13. S. Sun, C. Lv, W. Hong, X. Zhou, F. Wu, G. Chen, Dual Tuning of Composition and Nanostructure of Hierarchical Hollow Nanopolyhedra Assembled by NiCo-Layered Double Hydroxide Nanosheets for Efficient Electrocatalytic Oxygen Evolution, ACS Applied Energy Materials 2 (2019) 312−319.

14. L. Qian, Z. Lu, T. Xu, X. Wu, Y. Tian, Y. Li, Z. Huo, X. Sun, X. Duan, Trinary Layered Double Hydroxides as High-Performance Bifunctional Materials for Oxygen Electrocatalysis, Adv. Energy Mater. 5 (2015) 1500245.

15. C. Dong, X. Yuan, X. Wang, X. Liu, W. Dong, R. Wang, Y. Duan, F. Huang, Rational design of cobalt–chromium layered double hydroxide as a highly efficient electrocatalyst for water oxidation, J. Mater. Chem. A 4 (2016) 11292−11298.

16. M. Rinawati, Y.-X. Wang, K.-Y. Chen, M.-H. Yeh, Designing a spontaneously deriving NiFe-LDH from bimetallic MOF-74 as an electrocatalyst for oxygen evolution reaction in alkaline solution, Chem. Engin. J. 432 (2021) 130204.

17. X. Han, C. Yu, J. Yang, C. Zhao, H. Huang, Z. Liu, P. M. Ajayan, J. Qiu, Mass and Charge Transfer Coenhanced Oxygen Evolution Behaviors in CoFe-Layered Double Hydroxide Assembled on Graphene, Adv. Mater. Interfaces 3 (2016) 1500782.

18. T. Bhowmik, M. K. Kundu, S. Barman, CoFe Layered Double Hydroxide Supported on Graphitic Carbon Nitrides: An Efficient and Durable Bifunctional Electrocatalyst for Oxygen Evolution and Hydrogen Evolution Reactions, ACS Appl. Energy Mater. 3 (2018) 1200–1209.

19. Y. Lin, H. Wang, C.-K. Peng, L. Bu, C.-L. Chiang, K. Tian, Y. Zhao, J. Zhao, Y.-G. Lin, J.-M. Lee, L. Gao, Co-Induced Electronic Optimization of Hierarchical NiFe LDH for Oxygen Evolution, Small 16 (**2020)** e2002426.

20. H. Xu, B. Wang, C. Shan, P. Xi, O. W. Liu, O. Y. Tang, Ce-Doped NiFe-Layered Double Hydroxide Ultrathin Nanosheets/Nanocarbon Hierarchical Nanocomposite as an Efficient Oxygen Evolution Catalyst, ACS Appl. Mater. Interfaces 10 (2018) 6336–6345.

21. J. Zhang, J. Liu, L. Xi, Y. Fu, Y. N. Chen, S. Sun, W. Wang, K. M. Lange, B. Zhang, Single-Atom Au/NiFe Layered Double Hydroxide Electrocatalyst: Probing the Origin of Activity for Oxygen Evolution Reaction, J. Am. Chem. Soc. 140 (2018) 3876–3879.

22. J. Liu, Y. Ji, J. Nai, X. Niu, Y. Luo, L. Guo, S. Yang, Ultrathin amorphous cobalt–vanadium hydr(oxy)oxide catalysts for the oxygen evolution reaction, Energy Environ. Sci., 2018,11, 1736–1741.

23. M. Suliman, A. A. Ghamdi, T. Baroud, Q. Drmosh, M. Qamar, Growth of ultrathin nanosheets of nickel iron layered double hydroxide for the oxygen evolution reaction, Int. J. Hydrogen Energy 47 (**2022)** 23498–23507.

24. X. Wang, Y. He, Y. Zhou, R. Li, W. Liu, In situ growth of NiCoFe-layered double hydroxide through etching Ni foam matrix for highly enhanced oxygen evolution reaction, Int. J. Hydrogen Energy 47 (2022) 23644–23652.